HHS Public Access

Author manuscript

J Am Chem Soc. Author manuscript; available in PMC 2018 May 01.

Published in final edited form as:

J Am Chem Soc. 2017 September 13; 139(36): 12784–12792. doi:10.1021/jacs.7b07230.

The Oxidation State of [4Fe4S] Clusters Modulates the DNA-Binding Affinity of DNA Repair Proteins

Edmund C. M. Tse, **Theodore J. Zwang**, and **Jacqueline K. Barton***

Division of Chemistry and Chemical Engineering, California Institute of Technology, Pasadena, California 91125, United States

Abstract

A central question important to understanding DNA repair is how certain proteins are able to search for, detect, and fix DNA damage on a biologically relevant timescale. A feature of many base excision repair proteins is that they contain [4Fe4S] clusters that may aid their search for lesions. In this report, we establish the importance of the oxidation state of the redox-active [4Fe4S] cluster in the DNA damage detection process. We utilize DNA-modified electrodes to generate repair proteins with [4Fe4S] clusters in the 2+ and 3+ states by bulk electrolysis under an O_2-free atmosphere. Anaerobic microscale thermophoresis results indicate that proteins carrying $[4Fe4S]^{3+}$ clusters bind to DNA 550 times more tightly than those with $[4Fe4S]^{2+}$ clusters. The measured increase in DNA-binding affinity matches the calculated affinity change associated with the redox potential shift observed for [4Fe4S] cluster proteins upon binding to DNA. We further devise an electrostatic model that shows this change in DNA-binding affinity of these proteins can be fully explained by the differences in electrostatic interactions between DNA and the [4Fe4S] cluster in the reduced versus oxidized state. We then utilize atomic force microscopy (AFM) to demonstrate that the redox state of the [4Fe4S] clusters regulates the ability of two DNA repair proteins, Endonuclease III and DinG, to bind preferentially to DNA duplexes containing a single site of DNA damage (here a base mismatch) which inhibits DNA charge transport. Together, these results show that the reduction and oxidation of [4Fe4S] clusters through DNA-mediated charge transport facilitates long-range signaling between [4Fe4S] repair proteins. The redox-modulated change in DNA-binding affinity regulates the ability of [4Fe4S] repair proteins to collaborate in the lesion detection process.

Graphical Abstract

(top) DNA-mediated charge transport signaling is central to the first step of DNA damage detection and occurs only through well-matched but not mismatched (denoted as a red box) DNA duplexes between repair proteins (green and gray) carrying oxidized (orange) and reduced (purple) [4Fe4S] metallocofactors. (bottom) Upon the oxidation of the [4Fe4S] cluster from 2+ to 3+, the DNA binding affinity of the protein increases.

*Corresponding Author: jkbarton@caltech.edu.

Notes

The authors declare no competing financial interest.

Supporting Information

The Supporting Information is available free of charge on the ACS Publication website.

Supplementary Figures (Figures S1–13), Supplementary Tables (Tables S1–9), and Supplementary Experimental Procedures

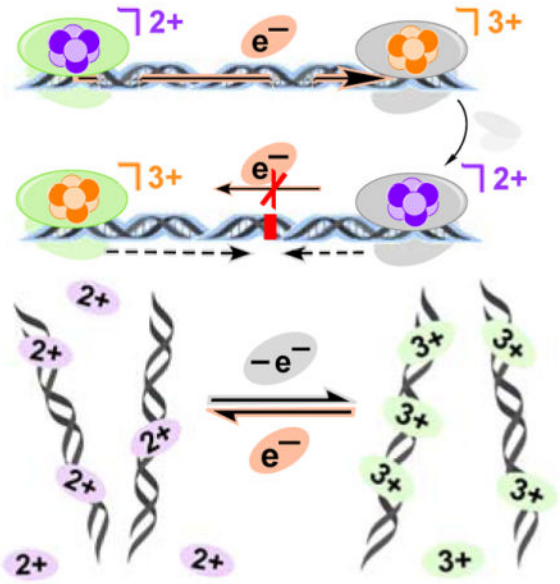

INTRODUCTION

Exogenous and endogenous damage to deoxyribonucleic acid (DNA), originating from sources such as reactive oxygen species, UV irradiation, and environmental mutagens, causes lesions, mismatches, and base pair modifications in the genome of organisms on the order of millions per cell per day.[1,2] Many repair mechanisms have evolved to uphold genome integrity by repairing DNA damage caused by oxidative stress.[3,4] DNA repair systems utilize diverse teams of proteins to respond, search, and repair DNA damage in a timely fashion. [5,6] An increasing number of DNA-processing enzymes, including many that are involved in the repair of DNA damage, have been found in archaea, bacteria, and eukaryotes to contain [4Fe4S] clusters.[7–10] Elucidating the role of these clusters remains an active area of investigation.[11–14] Initially, these clusters were proposed to serve primarily a role in maintaining protein structural integrity. However, recent experiments demonstrate that the presence of the [4Fe4S] cluster is not essential for the overall protein structure and thermal stability of a DNA repair enzyme, even though the cluster contributes significantly to DNA binding and enzymatic activity.[15] Other studies detailing processes loading iron-sulfur clusters into repair proteins indicate that these multistep assembling procedures are resource-intensive and suggest that these clusters may have other roles.[16–20]

Calculations have been performed to estimate the time needed for these [4Fe4S] repair proteins to search for DNA damage, and the results indicate that 3D random collisions, 2D sliding and hopping, and facilitated diffusion are not fast enough to explain the quick action of these proteins.[21] Given the low copy number of unique DNA-processing [4Fe4S] enzymes, ranging from 500 to as low as 10 per cell,[22,23] and the vast number of DNA lesions, we have proposed that these proteins aid one another through signaling using DNA-mediated charge transport (CT) between their [4Fe4S] clusters to search for and locate DNA damage sites more efficiently.[21,24,25]

The highly ordered π-stacking structure of aromatic bases enables efficient CT through double-stranded DNA (dsDNA).[26–28] One single base pair mismatch, lesion, or abasic site that disrupts π-stacking can attenuate DNA-mediated CT significantly.[29–31] Ground state CT mediated by dsDNA has been measured over 100 base pairs of length, and, given a very shallow distance dependence, there is no clear indication for the maximum distance that charge can move through dsDNA.[32]

Experiments with DNA repair proteins in the native 2+ oxidation state for the cluster show that CT-active proteins containing [4Fe4S] clusters localize in the vicinity of damage.[24,25,33] The DNA-mediated redox properties of [4Fe4S] proteins have been established *in vitro* using biochemical assays and DNA-modified electrodes. These experiments show that the [4Fe4S] cluster within a protein can be reduced to the 2+ state or oxidized to the 3+ state by CT through a DNA duplex. The efficiency of this process is diminished when the DNA contains a mismatch or abasic site located between the protein and the electrode.[29–31] Furthermore these experiments have found that binding to DNA shifts the $[4Fe4S]^{2+/3+}$ couple negative by about 200 mV to ca. +80 mV vs. NHE.[34,35] This shift thermodynamically suggests a corresponding shift in the DNA-binding affinity of proteins with an oxidized [4Fe4S] cluster by at least two orders of magnitude when compared to the reduced protein. However, no direct measurement of the DNA-binding affinities of [4Fe4S] repair proteins with intact clusters in both the reduced and oxidized state have been obtained. Also, it is unclear how much of this potential shift is caused by the change in affinity, as it may be influenced by a variety of other factors, such as a reorganization of residues in the local environment of the cluster. Thus, it is essential to measure directly the change in affinity associated with [4Fe4S] redox state.

In this report, we systematically vary the oxidation state of the [4Fe4S] cluster and measure how the redox state of the metallocofactor modulates DNA binding and, in turn, controls DNA damage detection activity of repair proteins. We specifically interrogate how oxidative stress influences the ability of [4Fe4S]-containing DNA repair proteins, Endonuclease III (EndoIII) and DinG, to bind preferentially to a 3 kilobase pairs (kbp) DNA duplex with a single-base mismatch *in vitro.* EndoIII is a base excision repair (BER) glycosylase that repairs oxidized pyrimidines in *Escherichia coli* (*E. coli*).[9] DinG is a DNA helicase that unwinds R-loops caused by invasion of DNA duplexes by nascent mRNA strands at transcription bubbles in *E. coli*.[36] Both proteins have been identified to contain high-potential [4Fe4S] clusters (HiPIPs), which cycle between the $[4Fe4S]^{3+}$ and $[4Fe4S]^{2+}$ states at physiological potentials when bound to dsDNA. Previous reports have demonstrated that EndoIII and DinG can interact with each other in a synergistic fashion by localizing on mismatch-containing DNA strands *in vitro* and rescuing *E. coli* growth *in vivo*.[33,37] Neither protein binds preferentially to a mismatch site, so the preference for binding the mismatch-containing strand is attributed instead to the ability of the mismatch to inhibit DNA CT.[21,25,38,39] Here, we selectively oxidize and reduce the [4Fe4S] metallocofactors in EndoIII and DinG using electrochemical methods instead of adding chemical reagents, which could damage the proteins and DNA strands. We then utilize atomic force microscopy (AFM) to examine the DNA-protein interactions with varying amounts of [4Fe4S] cluster oxidation. We further develop an electrostatic model based upon the electrostatic interactions between

DNA and [4Fe4S] cluster proteins to understand the change in protein binding with oxidation state.

EXPERIMENTAL SECTION

General Procedures

Chemicals were obtained from commercial sources (Sigma Aldrich, Fisher Scientific, VWR, and New England Biolabs) and used without further purification unless otherwise specified. Protein buffer (pH 7.5, 20 mM NaH_2PO_4, 100 mM NaCl, 5% glycerol, 1 mM EDTA) and DNA buffer (pH 7.0, 5 mM NaH_2PO_4, 50 mM NaCl) were prepared using Milli-Q water (>18 MΩ cm). Solutions were degassed and sparged with Ar overnight prior to conducting electrochemical experiments and preparing AFM samples inside an anaerobic chamber (Coy Lab Products). Experiments performed were replicated at least three times using different samples, and data presented are from representative trials.

Preparation of DNA-modified Electrodes for Electrochemical Studies

DNA sequences were prepared using phosphoramidites (Glen Research) on a DNA Synthesizer (Applied Biosystems 3400) or purchased from Integrated DNA Technologies and then purified by high performance liquid chromatorgraphy (HPLC, HP 1100, Agilent). Thiolated DNA was prepared according to established methods by modifying the 5′ end using a C6 S–S phosphoramidite.[32] Deprotection, purification, quantification, matrix-assisted laser desorption ionization (MALDI) characterization using a Autoflex MALDI TOF/TOF (Bruker), annealing of DNA, fabrication of Au electrodes, and preparation of the DNA-modified Au electrodes were performed as described previously.[32,40,41] The Au electrodes were assembled and then incubated in a solution (200 μL) of thiol-modified dsDNA (50 μM) in DNA buffer for 24 h at room temperature in the dark. The electrode modified with a monolayer of thiolated-DNA was then backfilled with mercaptohexanol (1 mM, 200 μL) for 45 min, washed three times with DNA buffer or protein buffer prior to adding protein samples to the DNA-modified Au surfaces.

DNA sequences used for EndoIII electrochemistry:[35] HS-C6-5′-GT GAG CTA ACG TGT CAG TAC-3′ 3′-CA CTC GAT TGC ACA GTC ATG-5′

DNA sequences used for DinG electrochemistry:[33] HS-C6-5′-GT GCT GCA ACG TGT CTG CGC-3′ 3′-CA CGA CGT TGC ACA GAC GCG AGA GCA GAC GTC AGA-5′

(HS-C6 = hexanethiol linker)

Protein Preparation and Characterization

Wild-type proteins (EndoIII and DinG) were prepared as described previously.[33] Crude proteins were harvested from cells and purified using fast protein liquid chromatography (FPLC, Bio-Rad) at 4 °C. Protein concentration was quantified based on the [4Fe4S] cluster absorbance (ε_{410} = 17000 M^{-1} cm^{-1})[42] using a 100 Bio UV-visible spectrophotometer (Cary, Agilent). Cluster loading was over 70%. Protein samples (5 μM) were sealed in Teflon-capped cuvettes under anaerobic condition and characterized at room temperature on a Model 430 circular dichroism spectrometer (Aviv). Continuous-wave electron

paramagnetic resonance (EPR) and pulse electron spin echo envelope modulation (ESEEM) experiments were conducted on an EMX X-band CW-EPR Spectrometer (Bruker) and an ELEXSYS-E580 X,Q-band Pulse EPR Spectrometer (Bruker) at 10 K with samples sealed in EPR tubes in the glove bag.

Electrochemistry

Electrochemical studies were performed as described previously.[34,41,42] Electrochemical experiments were carried out in a three-electrode set-up under an anaerobic atmosphere. The working electrode was a DNA-modified Au electrode, the counter electrode was a piece of freshly-polished Pt wire separated from the solution by an agarose gel tip filled with NaCl (3 M), and the reference electrode was a Ag/AgCl electrode stored in saturated NaCl solution modified with an agarose gel tip filled with NaCl (3 M). All redox potentials were converted to and reported versus the NHE scale.

Cyclic voltammetry, square wave voltammetry, and chronoamperometry were carried out using a 760 D Electrochemical Workstation (CH Instruments) at room temperature inside an anaerobic chamber. The atmosphere of the anaerobic chamber (< 1 ppm O_2, ca. 3.4% H_2) was monitored using a CAM-12 O_2 and H_2 sensor (Coy Lab Products). The chamber was maintained O_2-free by using two ventilated Pd catalyst packs (Coy Lab Products). Protein sample was placed on an electrode surface and successive potential cycling treatments between +0.4 V and −0.2 V vs. NHE at a scan rate of 100 mV/s using cyclic voltammetry were taken until the signal stabilizes. Bulk electrolytic oxidation and reduction of proteins were conducted by holding the electrode potential at +250 mV and −50 mV respectively vs. NHE for 25 min which is when the current stabilizes at a value similar to the background current obtained in a trial without protein in solution. The amount of charge passed during bulk electrolysis was cal3 culated by integrating the area under the background-subtracted curve in the current vs. time chronoamperometric plot. The integrated charge was then divided by the Faraday's constant (96485 C/mol) to convert to the total number of moles of electrons passed.[43] Since a [4Fe4S] cluster undergoes a 1-electron redox process,[44] the number of moles of electrons passed equals to the number of proteins oxidized or reduced. The number of moles of proteins present in the solution prior to bulk electrolysis was calculated from the molarity and volume of the protein solution used. The bulk electrolysis yield was then computed as the percentage of [4Fe4S] cluster protein oxidized or reduced in the whole protein sample.

Synthesis of DNA Strands for AFM Experiments

Short well-matched DNA duplex, long well-matched DNA duplex, and long DNA duplex with a C:A mismatch engineered in the middle were prepared using published protocols.[21,25,33] Briefly, four primers were synthesized, phosphorylated, and purified using phenol–chloroform extraction followed by ethanol precipitation. After drying under vacuum overnight, primers were used in PCR reactions using pUC19 as a template to generate two DNA duplexes containing 14-nucleotide single-strand overhang. Short and long duplexes were annealed and ligated together. Incomplete reaction resulted in a mixture of ligated (3767 bp, ca. 1.2 μm in length) and unligated (1610 bp and 2157 bp, ca. 0.5 μm and 0.7 μm in length) dsDNA samples that were identical with the exception of the presence of the

mismatch site engineered at the overhang region. The single-strand overhang of unligated dsDNA was conjugated to complementary DNA strands prior to AFM experiments.

AFM Experiments

AFM was conducted following protocol reported previously.[21,25,33] Briefly, mica surfaces were freshly cleaved with tape. Protein stock solution containing either 5 μM EndoIII or 2 μM DinG was collected after bulk electrolysis. Stock DNA solution (6 ng/μL) contained the mixture of ligated duplexes and the two unligated duplexes in Tris elution buffer (EB, Qiagen). A solution with a final protein concentration (12 nM) and a final DNA concentration (1 ng/μL) was prepared and incubated at room temperature for 1 h to allow for the loading of protein onto DNA to reach equilibrium under an anaerobic atmosphere and minimize cluster degradation. $MgCl_2$ (200 mM, 1.5 μL per 25 μL total volume) was added to promote DNA adsorption on mica for AFM experiments. After pipetting 10 μL of DNA/protein/$MgCl_2$ solution onto a mica surface and incubating for 2 min, a continuous stream of deoxygenated Milli-Q water (2 mL) was slowly poured over the top portion of the modified mica surface while holding the piece of mica in a vertical position to linearize the DNA. A piece of kimwipe was used to dab dry the bottom edge of the mica surface. The surface was dried using a stream of N_2 flowing in the same direction as the water rinse for 2 min. pUC19 (2,686 bp, ca. 0.9 μm) linearized by HindIII (New England Biolabs) was used instead of the ligated and unligated DNA to quantify how the DNA-binding activity of EndoIII changes as a function of the ratio of oxidized $[4Fe4S]^{3+}$ cluster in the protein sample.

AFM Instrumentation

FESPA-V2 AFM tapping mode probes (Bruker Nano, Inc.) with a mean force constant of 2.8 N/m and mean resonance frequency of 75 kHz were used in a MFP-3D AFM (Asylum Research). Images were captured in air with scan areas of 3×3 μm^2 in tapping mode at a scan rate of 1 Hz in order to obtain images of quality high enough for AFM redistribution assay analysis (512 pixels/line, 512 lines/image). The images were collected and analyzed blind.

Differential Binding Density Ratio Calculations

WSxM software (Igor Pro) was used to measure DNA contour lengths and height profiles of the proteins as described previously. [21,25,33] DNA and proteins were identified using the relative differential height profiles between protein and DNA. For each data set, images from at least three independent samples were analyzed, compared, and pooled (> 400 long and short duplexes). Distinguishable DNA and proteins were counted by hand. Duplexes that were overlapped, indistinguishable, or cut off by the edge of the image were excluded from our counting procedure. For each sample, the binding density ratio, *r*, (see Eq. 1) is defined as the ratio of the proteins bound on long duplexes divided by proteins bound on short duplexes, which serve as an internal normalization factor to correct changes in concentration across samples that may confound results. Data presented are from representative trials, and error bars represent standard error of all trials based on the total number of proteins observed (n > 200 for all experiments). The differential binding density ratio, *dr*, (see Eq. 2) is calculated by dividing the *r* from the mismatched sample by the *r* from the well-matched sample.

$$r = \frac{\#\ of\ proteins\ on\ long\ duplexes}{\#\ of\ proteins\ on\ short\ duplexes} \quad \text{Eq. 1}$$

$$dr = \frac{r_{mismatched}}{r_{well-matched}} = \frac{\left(\frac{\#\ of\ proteins\ on\ mismatched\ long\ duplexes}{\#\ of\ proteins\ on\ short\ duplexes}\right)}{\left(\frac{\#\ of\ proteins\ on\ well-matched\ long\ duplexes}{\#\ of\ proteins\ on\ short\ duplexes}\right)} \quad \text{Eq. 2}$$

Microscale Thermophoresis

Microscale thermophoresis (MST) was carried out using a Monolith NT.115 series instrument (NanoTemper) at 21 °C. Oligonucleotides (21 bp in length) based on the DNA sequence used in the AFM studies were synthesized and annealed to generate well-matched DNA of 21 bp in length. For measurements of EndoIII primarily in the reduced state, native EndoIII with His_6-tag (200 nM, 100 μL) was mixed with MO-L008 His-tag labeling kit RED-tris-NTA (100 nM, 100 μL, NanoTemper) for 30 min at room temperature. The sample was centrifuged at 4 °C and 15,000 g for 10 min. Serial dilution of dsDNA as titrants was performed in PCR 8-strip tubes with individual caps (USA Scientific) following the user manual provided by NanoTemper. Labeled protein (50 nM) was mixed with DNA titrant in the dark for 10 min. Samples with a final dye concentration of 25 nM were then loaded into MO-K003 Monolith NT.115 hydrophobic capillaries (NanoTemper) and were measured at 60% LED and 40% MST power. DNA buffer with 0.05% Tween 20 was used for MST studies. For measurements of EndoIII primarily in the oxidized state, EndoIII (1 μM, 200 μL) was oxidized in the absence of O_2 using DNA-modified electrode previously described. Oxidized EndoIII was labeled with RED-tris-NTA under anaerobic condition in an aluminum-wrapped Eppendorf tube. MST samples were loaded into hydrophobic capillary tubes inside a glove bag in the dark. Capillaries were sealed with HR4-328 capillary wax (Hampton Research) using a hand-held wax pen (Hampton Research) in the absence of O_2 and light.

DNA sequences used for MST measurements: 5′-ACT GAA CTC TGT ACC TGG CAC-3′ 3′-TGA CTT GAG ACA TGG ACC GTG-5′

Electrostatic Modeling

Distances between the [4Fe4S] cluster of EndoIII and the phosphate groups on the backbone of the DNA-bound EndoIII in the native state were obtained from a published crystal structure (PDB: 1ORN).[45] The 1ORN crystal structure also provided the number of phosphates interacting with protein residues. The dielectric constant of the portion of EndoIII of interest was estimated by calculating the average dielectric constant of the amino acid residues[46] surrounding the [4Fe4S] cluster and in between the [4Fe4S] cluster and the bound DNA strand. In this electrostatic model, the [4Fe4S] cluster and the phosphate groups

on the DNA backbone were modeled as point charges. The potential energy (PE) between two charged particles was calculated using Eq. 3

$$PE = \frac{(q_1)(q_2)}{4\pi\varepsilon_0\varepsilon_r d} \quad \text{Eq. 3}$$

with q = charge, ε_0 = permittivity of free space, ε_r = dielectric constant, and d = distance between charges. The difference in PE between EndoIII in the reduced and oxidized states was computed by calculating the difference between the total PE for the $[4Fe4S]^{3+}$ case and the total PE for the $[4Fe4S]^{2+}$ case. The experimental energy difference between the 3+ case and the 2+ case was calculated using the Nernst equation by converting the redox potential shift recorded using electrochemical techniques.[34] The electrostatic model was supported by comparing the modeled PE and the experimental energy difference.

RESULTS

Oxidation and Reduction of [4Fe4S] Proteins using Electrochemical Methods

Cyclic voltammetry (CV) was used to investigate the electrochemical properties of EndoIII on DNA-modified Au electrodes (Figure 1). These data, along with square wave voltammetry and differential pulse voltammetry measurements (Figures S1–2) show that within our potential window EndoIII exhibits a single redox couple with a DNA-bound midpoint potential of about +80 mV vs NHE, consistent with previous measurements of the $[4Fe4S]^{2+/3+}$ redox couple in EndoIII when associated to DNA.[34,35,39]

Solutions of primarily reduced or primarily oxidized EndoIII with an intact [4Fe4S] cluster were generated using bulk electrolysis and confirmed using electron paramagnetic resonance (EPR) and circular dichroism (CD). Randles-Sevcik analysis (Figures S3–4) demonstrates that there is exchange between proteins in solution and on the surface of the DNA-modified electrode so that a constant applied potential could oxidize or reduce the majority of proteins in the sample. The CVs shown in Figure 1 identify potentials at which the [4Fe4S] clusters of the proteins can be oxidized or reduced, which allow us to conduct bulk electrochemical oxidation and reduction of EndoIII at +250 mV and −50 mV vs. NHE, respectively. Similar electrolysis experiments were utilized to examine primase using its [4Fe4S] cluster as a redox switch.[47] Figure 1 also shows the oxidation of EndoIII on a DNA-modified electrode held at a constant potential for 25 min to drive electrolysis to completion. Applying an oxidizing or reducing potential to a solution with protein present results in a larger magnitude current than measured in the buffer control (Figure S5). This difference is indicative of the proteins being oxidized or reduced on the DNA-modified electrode surface, and the current decreases over time as the oxidation or reduction approaches completion (> 99% yield). We then utilized EPR to characterize the reduced and oxidized EndoIII generated by bulk electrolysis (Figure S6). The reduced EndoIII is EPR-silent and the oxidized EndoIII exhibits an EPR signal with a g value of 2.07, which are consistent with intact $[4Fe4S]^{2+}$ and $[4Fe4S]^{3+}$ clusters, respectively.[48]

Binding Affinity Measurements Comparing EndoIII with Oxidized and Reduced [4Fe4S] Cluster

AFM was used to explore how the DNA-binding activity of EndoIII changes as the amount of oxidized and reduced clusters in the protein sample was varied (Figure 2). We then recorded the number of EndoIII present on the linearized pUC19 plasmid DNA as a function of the proportion of oxidized $[4Fe4S]^{3+}$ cluster in the protein sample (Table S1). As the ratio of EndoIII with oxidized $[4Fe4S]^{3+}$ metallocofactors increases, the number of EndoIII bound on DNA increases (Figure 2). This trend indicates that oxidized EndoIII binds more tightly to DNA than does the reduced protein. We then utilized electrophoretic mobility shift assay (EMSA), isothermal titration calorimetry (ITC), and microscale thermophoresis (MST) to probe the non-specific DNA-binding affinity of EndoIII to well-matched dsDNA of 21 bp in length. In all three cases, we observed an increase in binding affinity of EndoIII to dsDNA upon oxidizing the [4Fe4S] metallocofactor from the 2+ state to the 3+ state (Table 1). However, ITC is not anaerobic and EMSA generates O_2 *in situ*, both of which result in cluster degradation that prevent accurate binding affinity measurements (see S.I. for further discussion). To prevent cluster degradation, we utilized MST for anaerobic binding affinity measurement.[49] MST results show that EndoIII predominantly in the reduced state exhibits a K_D of 6.1 μM ± 0.9 μM for unmodified duplex DNA and EndoIII predominantly in the oxidized state displays a K_D of 0.011 μM ± 0.002 μM (Figures 3 and S7). Thus, we observed a 550 ± 130 times increase in DNA-binding affinity of EndoIII upon oxidation, which further supports the trend observed using AFM that the EndoIII occupancy on DNA increases upon oxidation.

Electrostatic DNA-Protein Binding Model

To understand the origin of the redox-modulated affinity, we developed an electrostatic model that investigates the perturbation in the electrostatic interactions between DNA and proteins upon the addition or removal of an electron at the [4Fe4S] metallocofactor (Figure S8). This electrostatic model incorporates atomic distances obtained from crystallographic data and knowledge regarding the DNA-binding pocket from published literature.[9,45,50] The crystal structure (PDB: 1ORN) revealed that eight negatively-charged phosphates on the DNA backbone not bound by cations interact with the amino acid residues of EndoIII. Another crystallographic study demonstrated that a high-potential iron-sulfur protein (HiPIP) undergoes only minor structural changes upon toggling the redox state of the [4Fe4S] cluster between 2+ and 3+.[51] Therefore, we assumed the coordinates of the atoms in the EndoIII protein structure are the same for both the $[4Fe4S]^{3+}$ and $[4Fe4S]^{2+}$ cases. The binding energy resulting from electrostatic interactions between the positively charged [4Fe4S] cluster and the negatively-charged phosphate groups on the DNA backbone are calculated to be ca. 7 kcal/mol, comparable to the energy change measured from the redox potential shift of EndoIII upon binding DNA using the Nernst equation, ca. 5 kcal/mol.[52] The model ΔPE for MutY also recapitulates the energy difference between the 2+ and 3+ states computed from the redox potential shift obtained using electrochemical techniques.[35] This result emphasizes that our electrostatic model is general and is readily applicable to other DNA-processing enzymes carrying [4Fe4S] metallocofactors. This model shows that the difference in binding affinity for the two oxidation states, $[4Fe4S]^{2+}$ and $[4Fe4S]^{3+}$, can

be explained primarily by the electrostatic interactions between the cluster and DNA without a substantial protein structural change.

Signaling Between Oxidized and Reduced EndoIII to Search for DNA Damage

We then examined the effect of the redox state of the [4Fe4S] metallocofactor on the ability of EndoIII to differentiate between well-matched (WM) and mismatched (MM) DNA strands by AFM. Solutions of EndoIII with controlled amounts of oxidized $[4Fe4S]^{3+}$ cluster and reduced $[4Fe4S]^{2+}$ cluster were incubated with two different mixtures of DNA and then the two sets of AFM results were compared. The first DNA mixture contained long and short duplexes with no mismatches, while the second DNA mixture contained both short DNA duplexes with no mismatches and long DNA duplexes with a single C:A mismatch, which is not a native substrate for EndoIII but does inhibit DNA CT, engineered in the middle of the strand. The short WM DNA duplexes are identical in the two sets of experiments so the binding distribution profiles across the two data sets can be normalized and compared to one another (Tables S2–3). Figure 4 shows a bar graph summarizing the ability for solutions of EndoIII with varying proportions of oxidized proteins to bind preferentially to DNA with a single-base mismatch. Here we observed that the ability for EndoIII to differentiate between MM and WM DNA strands decreases as the percentage of oxidized protein in the sample increases. It should be noted that these data could also be used to determine the change in binding affinity with oxidation. On this basis, we found a 4–30 fold increase in DNA-binding affinity upon oxidizing the [4Fe4S] cluster of EndoIII. The trend observed is consistent with that obtained using other techniques, but the magnitude of change is significantly smaller. This difference likely can be attributed to the protein-DNA sample not being at equilibrium in the AFM experiment, because of kinetic limitations associated with tight DNA binding, precluding rapid, full redistribution of proteins along the DNA.

Signaling Between EndoIII and DinG to Search for DNA Damage

This change in binding density ratio, associated with a change in oxidation state, could be used as a diagnostic of oxidation state in the AFM experiment and therefore a means to identify redox signaling between proteins. We evaluated whether DinG, another DNA-processing enzyme containing a [4Fe4S] cluster, exhibits the same redox-modulated ability as EndoIII to bind preferentially to DNA duplexes with an intervening lesion. We chose to incorporate DinG because it has been shown to carry out DNA signaling with EndoIII; both proteins in the native oxidation state search for DNA damage *in vitro* and there is evidence that EndoIII helps DinG rescue defective growth *in vivo*.[33] DinG exhibits a DNA-bound redox potential comparable to that of EndoIII (Figures S9–12). We subjected DinG to bulk electrolysis conditions similar to EndoIII to generate DinG with intact oxidized and reduced [4Fe4S] metallocofactors (Figure S13). Analogous to EndoIII, oxidizing DinG decreases its ability to bind preferentially to DNA duplexes with a single-base mismatch (Figure 5 and Tables S4–5).

Mixtures of reduced DinG and oxidized EndoIII, as well as mixtures of oxidized DinG and reduced EndoIII, were then prepared to address whether a reduced protein can signal with a different oxidized protein (Tables S6–9). This cross experiment includes four scenarios: two

contain proteins at the 33% overall oxidized state, and two contain proteins at the 66% overall oxidized state. Figure 5 shows the results of the cross experiments. When the overall protein oxidation is either 33% and 66%, EndoIII and DinG exhibit intermediate binding density ratios in between the values obtained for predominantly reduced and predominantly oxidized protein samples. These findings demonstrate that reduced proteins from different repair pathways can undergo DNA-mediated redox signaling with oxidized proteins to collaboratively search for and preferentially bind to DNA duplexes with a single-base mismatch.

DISCUSSION

Redox-Active [4Fe4S] Cluster of Repair Proteins Functions as a DNA-Binding Affinity Switch

Non-specific binding to DNA is an important first step in the damage search and repair process.[3–5,24] The binding affinity measurements reported in this work clearly indicate that the oxidized protein has an increased binding affinity for DNA relative to the reduced protein. This direct measurement of an increased affinity is consistent with electrochemical results that previously demonstrated binding to DNA shifts the redox potential of the $[4Fe4S]^{2+/3+}$ couple of the cluster negative by about 200 mV,[35,53,54] which indirectly showed that oxidation increases the protein/DNA binding affinity by at least two orders of magnitude.[34]

We devised an electrostatic model to understand the underlying chemistry that dictates the apparent change in DNA-binding affinity. We assumed that changing redox state of the [4Fe4S] cluster does not significantly alter the structure of the protein, consistent with minimal structural changes observed in recent crystallographic studies on a HiPIP that is reduced or oxidized,[51] EndoIII with and without DNA,[9,45,50] and MutY spectroscopically examined with and without a cluster.[15] Utilizing these structural data, we developed an electrostatic model to understand how the redox state of the [4Fe4S] cluster affects the charge-charge interaction. Crystallographic data confirms that EndoIII binds to the negatively-charged phosphate groups on the DNA backbone via a series of positively-charged residues.[45] Our electrostatic model is general and is readily applicable to other DNA-processing enzymes carrying [4Fe4S] metallocofactors. Our model demonstrates that the redox-modulated DNA-binding affinity can be fully explained by the electrostatic interactions between the [4Fe4S] cluster and the phosphate groups on the DNA backbone without a significant structural change between oxidized and reduced DNA-bound forms. The lack of a necessary conformational change may be critical in the detection and location of lesions.

Redox-Modulated DNA-Binding Affinity of [4Fe4S] Repair Proteins Regulates DNA-mediated CT Signaling

AFM experiments reveal that the oxidation state of the [4Fe4S] cluster influences the ability of the protein to localize on DNA duplexes with single-base mismatches. The total amount of oxidation is important for the efficiency of this DNA damage sensing process. Despite starting with oxidized protein that is unable to localize preferentially on mismatch-

containing DNA, the addition of reduced protein with different enzymatic function is able to achieve preferential binding. Intriguingly, the amount of oxidized [4Fe4S] cluster among all proteins in a mixture is a better predictor of damage recognition than the identity of the proteins with initially reduced or oxidized [4Fe4S] metallocofactors; thus it can be used as a diagnostic of signaling between proteins.

To mimic cellular oxidative stress, our group previously used H_2O_2 to oxidize the [4Fe4S] cluster in EndoIII. These experiments found that H_2O_2 increases the preference of [4Fe4S] cluster proteins for DNA duplexes containing a mismatch. [21] These results are fully consistent with the idea that repair proteins with $[4Fe4S]^{2+}$ clusters sense and respond to oxidative stress via cluster oxidation to the 3+ state. However, it is unclear what other effects the H_2O_2 may have on the proteins and DNA in this system.[5,24] The use of chemical oxidants such as $K_3Fe(CN)_6$ and H_2O_2 degrade [4Fe4S] clusters.[6,42] Also, the oxidation extent of the [4Fe4S] cluster in the protein sample cannot be accurately quantified by using an excess amount of H_2O_2 as the oxidant. The electrochemical oxidation and reduction presented here provides a milder and well-controlled condition that allows for changing the redox state of [4Fe4s] clusters. Together, these data confirm that oxidative stress can generate repair proteins with $[4Fe4S]^{3+}$ clusters that can aid the DNA damage search. It is important to note that the short incubation time in both of these experiments, which was required for sample stability, means that the protein-DNA binding may not be at equilibrium. If anything, giving more time to equilibrate should result in higher preferential binding to the duplex with the mismatch.

These observations using AFM are consistent with a DNA damage search scheme based on DNA-mediated redox signaling between proteins with oxidized and reduced [4Fe4S] clusters (Figure 5). DNA-mediated CT can occur between two proteins and, our data shows conclusively, this CT results in a change in affinity for each of the proteins. Incorporating a single C:A mismatch within a DNA duplex, even though it is not a preferred substrate for either EndoIII or DinG,[27,31] is able to increase the number of proteins bound to that duplex relative to a duplex with no mismatches. In these experiments the mismatch only serves to disrupt DNA CT between proteins and, therefore, DNA CT prevents the exchange of affinity that results from changing the redox state of the [4Fe4S] clusters. This change in redox state increases the effective affinity of these proteins for a duplex containing a mismatch because it allows for oxidized proteins to stay in the vicinity of the mismatch, or potentially any lesion that disrupts DNA CT, without being reduced and released from the duplex by another protein. These data bolster the claim that proteins, even with completely different cellular roles, can work in concert to aid their search for DNA damage by reducing and oxidizing one another via long-range CT through DNA.[55–57]

Redox-Signaling Damage Search Model

DNA-mediated CT significantly expedites the search for DNA damage. Charge can be transported through large regions of DNA much faster than proteins can translocate, especially when the nuclear medium and DNA itself are crowded by other proteins. [21] If a high-affinity, oxidized protein is bound to a region with no lesion, the protein may quickly become reduced by another protein along the duplex, and the decreased affinity will allow

for it to release DNA and scan elsewhere (Figure 5). If, however, there is a lesion disrupting DNA CT, the protein will remain oxidized and associated to DNA. They can utilize both DNA CT and translocation making the search process faster and more efficient.

DNA-Mediated Redox Signaling Enables Low Copy Number Proteins to Efficiently Find Their Substrate

A growing number of proteins that process DNA have been discovered to contain redox-active [4Fe4S] clusters.[7–10,20] Our data show that the oxidation state of the [4Fe4S] clusters is integral to the ability of proteins to search for DNA damage, but that the identity of the protein is unimportant for DNA-CT. The DNA-binding affinity depends on the oxidation state of the [4Fe4S] cluster in both EndoIII and DinG and likely holds true for other [4Fe4S] proteins. Intriguingly, this model suggests that DNA-processing proteins with different enzymatic functions may collaborate with each other to find damage so long as the [4Fe4S] clusters are in different redox states. Because the redox-modulated affinity relies purely on a change in electrostatic interactions and not on protein-specific changes in structure, the DNA-mediated redox signaling strategy between proteins containing [4Fe4S] clusters likely benefits the efficien9 cy of all DNA-processing proteins containing [4Fe4S] to find and repair damage.

Supplementary Material

Refer to Web version on PubMed Central for supplementary material.

Acknowledgments

We gratefully recognize the NIH (GM61077) for financial support. E.C.M.T. appreciates the Croucher Foundation for a post-doctoral fellowship. T.J.Z. is an NSF fellow (DGE-1144469). E.C.M.T. also thanks Zhou for assisting in the protein purification process and Dr. Deng for providing Au working electrodes. We are also grateful to the Caltech Center for the Chemistry of Cellular Signaling for instrumentation.

References

1. Jackson SP, Bartek J. Nature. 2009; 461:1071–1078. [PubMed: 19847258]
2. Lindahl T, Barnes DE. Cold Spring Harbor Symp Quant Biol. 2000; 65:127–134. [PubMed: 12760027]
3. Sancar A, Lindsey-Boltz LA, Unsal-Kacmaz K, Linn S. Annu Rev Biochem. 2004; 73:39–85. [PubMed: 15189136]
4. Marteijn JA, Lans H, Vermeulen W, Hoeijmakers JHJ. Nat Rev Mol Cell Biol. 2014; 15:465–481. [PubMed: 24954209]
5. David SS, O'Shea VL, Kundu S. Nature. 2007; 447:941–950. [PubMed: 17581577]
6. Hoeijmakers JHJ. Nature. 2001; 411:366–374. [PubMed: 11357144]
7. Fuss JO, Tsai CL, Ishida JP, Tainer J. BBA-Mol Cell Res. 2015; 1853:1253–1271.
8. Rouault TA. Nat Chem Biol. 2015; 11:442–445. [PubMed: 26083061]
9. Kuo C, McRee D, Fisher C, O'Handley S, Cunningham R, Tainer J. Science. 1992; 258:434–440. [PubMed: 1411536]
10. Fan L, Fuss JO, Cheng QJ, Arvai AS, Hammel M, Roberts VA, Cooper PK, Tainer JA. Cell. 2008; 133:789–800. [PubMed: 18510924]
11. Lukianova OA, David SS. Curr Opin Chem Biol. 2005; 9:145–151. [PubMed: 15811798]

12. Veatch JR, McMurray MA, Nelson ZW, Gottschling DE. Cell. 2009; 137:1247–1258. [PubMed: 19563757]
13. Saxena N, Maio N, Crooks DR, Ricketts CJ, Yang Y, Wei MH, Fan TWM, Lane AN, Sourbier C, Singh A, Killian JK, Meltzer PS, Vocke CD, Rouault TA, Linehan WM. J Natl Cancer Inst. 2016; 108:djv287.
14. Wu Y, Suhasini AN, Brosh RM. Cell Mol Life Sci. 2009; 66:1209–1222. [PubMed: 19099189]
15. Golinelli MP, Chmiel NH, David SS. Biochemistry. 1999; 38:6997–7007. [PubMed: 10353811]
16. Lill R. Nature. 2009; 460:831–838. [PubMed: 19675643]
17. Stehling O, Vanshisht AA, Mascarenhas J, Jonsson ZO, Sharma T, Netz DJ, Pierik AJ, Wohlschlegel JA, Lill R. Science. 2012; 337:195–199. [PubMed: 22678362]
18. Gari K, León Ortiz AM, Borel V, Flynn H, Skehel JM, Boulton SJ. Science. 2012; 337:243–245. [PubMed: 22678361]
19. Rouault TA. Nat Rev Mol Cell Biol. 2015; 16:45–55. [PubMed: 25425402]
20. Rouault TA. Dis Model Mech. 2012; 5:155–164. [PubMed: 22382365]
21. Boal AK, Genereux JC, Sontz PA, Gralnick JA, Newman DK, Barton JK. Proc Natl Acad Sci USA. 2009; 106:15237–15242. [PubMed: 19720997]
22. Demple B, Harrison L. Annu Rev Biochem. 1994; 63:915–948. [PubMed: 7979257]
23. Li G-W, Burkhardt D, Gross C, Weissman Jonathan S. Cell. 2014; 157:624–635. [PubMed: 24766808]
24. O'Brien E, Silva RMB, Barton JK. Isr J Chem. 2016; 56:705–723. [PubMed: 28090121]
25. Sontz PA, Mui TP, Fuss JO, Tainer JA, Barton JK. Proc Natl Acad Sci USA. 2012; 109:1856–1861. [PubMed: 22308447]
26. Genereux JC, Barton JK. Chem Rev. 2010; 110:1642–1662. [PubMed: 20214403]
27. Kelley SO, Jackson NM, Hill MG, Barton JK. Angew Chem Int Ed. 1999; 38:941–945.
28. Guo X, Gorodetsky AA, Hone J, Barton JK, Nuckolls C. Nat Nanotechnol. 2008; 3:163–167. [PubMed: 18654489]
29. Boal AK, Barton JK. Bioconjugate Chem. 2005; 16:312–321.
30. Bhattacharya PK, Barton JK. J Am Chem Soc. 2001; 123:8649–8656. [PubMed: 11535068]
31. Boon EM, Livingston AL, Chmiel NH, David SS, Barton JK. Proc Natl Acad Sci USA. 2003; 100:12543–12547. [PubMed: 14559969]
32. Slinker JDM, NB, Renfrew SE, Barton JK. Nat Chem. 2011; 3:230–235.
33. Grodick MA, Segal HM, Zwang TJ, Barton JK. J Am Chem Soc. 2014; 136:6470–6478. [PubMed: 24738733]
34. Gorodetsky AA, Boal AK, Barton JK. J Am Chem Soc. 2006; 128:12082–12083. [PubMed: 16967954]
35. Bartels PL, Zhou A, Arnold AR, Nuñez NN, Crespilho FN, David SS, Barton JK. Langmuir. 2017; 33:2523–2530. [PubMed: 28219007]
36. Boubakri H, de Septenville AL, Viguera E, Michel B. EMBO J. 2010; 29:145–157. [PubMed: 19851282]
37. Grodick MA, Muren NB, Barton JK. Biochemistry. 2015; 54:962–973. [PubMed: 25606780]
38. O'Handley S, Scholes CP, Cunningham RP. Biochemistry. 1995; 34:2528–2536. [PubMed: 7873533]
39. Boal AK, Yavin E, Lukianova OA, O'Shea VL, David SS, Barton JK. Biochemistry. 2005; 44:8397–8407. [PubMed: 15938629]
40. Slinker JD, Muren NB, Gorodetsky AA, Barton JK. J Am Chem Soc. 2010; 132:2769–2774. [PubMed: 20131780]
41. Kelley SO, Barton JK, Jackson NM, Hill MG. Bioconjugate Chem. 1997; 8:31–37.
42. Cunningham RP, Asahara H, Bank JF, Scholes CP, Salerno JC, Surerus K, Munck E, McCracken J, Peisach J, Emptage MH. Biochemistry. 1989; 28:4450–4455. [PubMed: 2548577]
43. Bard, AJ., Faulkner, LR. Electrochemical Methods: Fundamentals and Applications. Wiley; New York: 2000.
44. Venkateswara Rao P, Holm RH. Chem Rev. 2004; 104:527–560. [PubMed: 14871134]

45. Fromme JC, Verdine GL. EMBO J. 2003; 22:3461–3471. [PubMed: 12840008]
46. Li L, Li C, Zhang Z, Alexov E. J Chem Theory Comput. 2013; 9:2126–2136. [PubMed: 23585741]
47. O'Brien E, Holt ME, Thompson MK, Salay LE, Ehlinger AC, Chazin WJ, Barton JK. Science. 2017; 355:813–822.
48. Agarwalla S, Stroud RM, Gaffney BJ. J Biol Chem. 2004; 279:34123–34129. [PubMed: 15181002]
49. Webert H, Freibert SA, Gallo A, Heidenreich T, Linne U, Amlacher S, Hurt E, Mühlenhoff U, Banci L, Lill R. Nat Commun. 2014; 5:5013. [PubMed: 25358379]
50. Thayer MM, Ahern H, Xing D, Cunningham RP, Tainer JA. EMBO J. 1995; 14:4108–4120. [PubMed: 7664751]
51. Ohno H, Takeda K, Niwa S, Tsujinaka T, Hanazono Y, Hirano Y, Miki K. PLoS ONE. 2017; 12:e0178183. [PubMed: 28542634]
52. Atkins, P., de Paula, J. Atkins' Physical Chemistry. OUP; Oxford: 2010.
53. Boon EM, Pope MA, Williams SD, David SS, Barton JK. Biochemistry. 2002; 41:8464–8470. [PubMed: 12081496]
54. Boal AK, Yavin E, Barton JK. J Inorg Biochem. 2007; 101:1913–1921. [PubMed: 17599416]
55. Merino EJ, Boal AK, Barton JK. Curr Opin Chem Biol. 2008; 12:229–237. [PubMed: 18314014]
56. Arnold AR, Grodick MA, Barton JK. Cell Chem Biol. 2016; 23:183–197. [PubMed: 26933744]
57. Genereux JC, Boal AK, Barton JK. J Am Chem Soc. 2010; 132:891–905. [PubMed: 20047321]

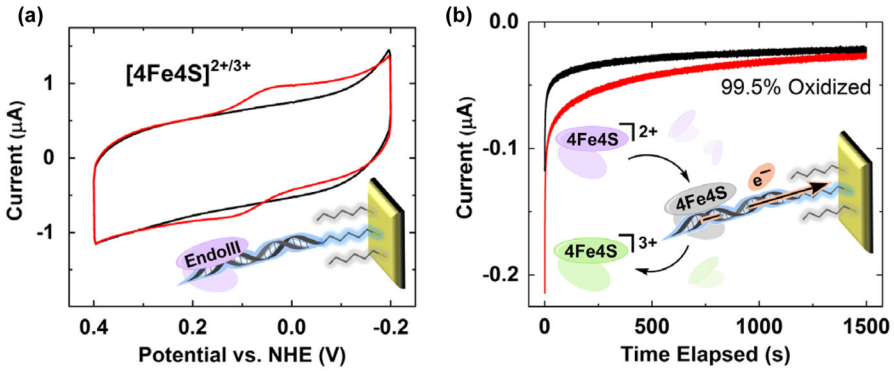

Figure 1.

Electrochemistry of EndoIII on DNA-modified electrodes. (a) CVs at a scan rate of 100 mV/s and (b) bulk electrolysis held at +250 mV vs. NHE in DNA buffer (pH 7.0, 5 mM NaH_2PO_4, 50 mM NaCl) without (black) and with 1 μM EndoIII (red) using DNAmodified electrodes passivated with mercaptohexanol.

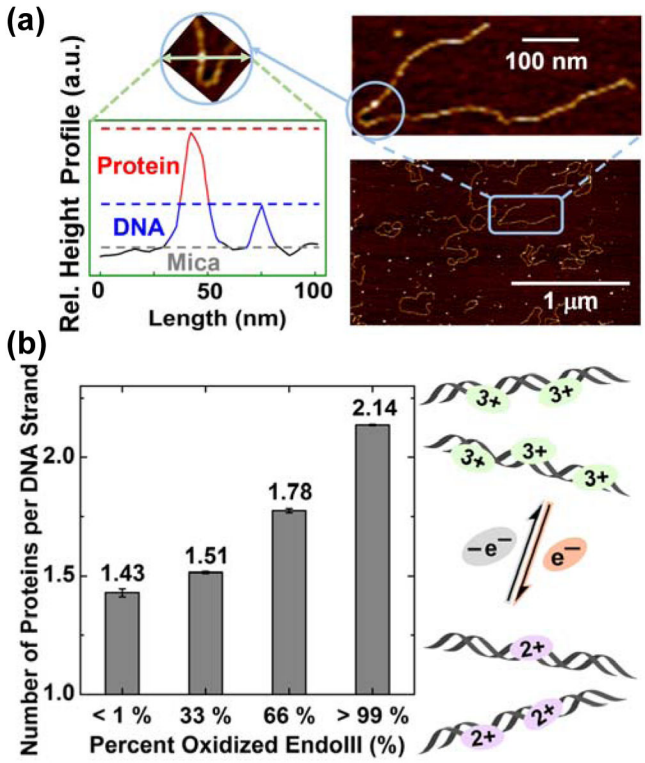

Figure 2.

AFM visualization of EndoIII binding to DNA. (a) Visualization of proteins on DNA duplexes using AFM. The relative height of proteins allows for them to be distinguished from DNA and counted. (b) Plot of the amount of EndoIII bound on a DNA strand as a function of the extent of oxidation of the protein samples. The 33% and 66% oxidized EndoIII samples were prepared by mixing reduced and oxidized EndoIII in a 2:1 and 1:2 ratios, respectively. Curved lines in the schematic on the right represent linearized pUC19 DNA duplexes.

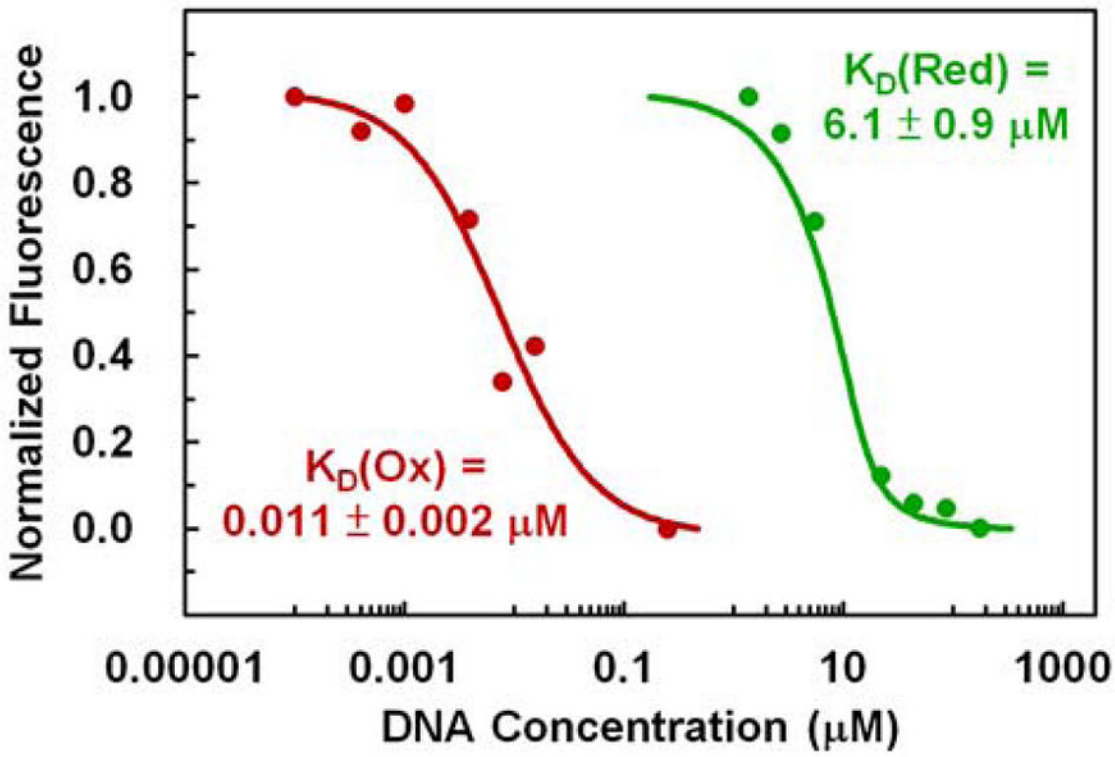

Figure 3.

Microscale thermophoresis (MST) results of EndoIII. MST plots of reduced (green) and oxidized (red) EndoIII binding to DNA. A 21-mer duplex was used as the titrant. A 550-fold increase in binding affinity was observed for EndoIII upon oxidation.

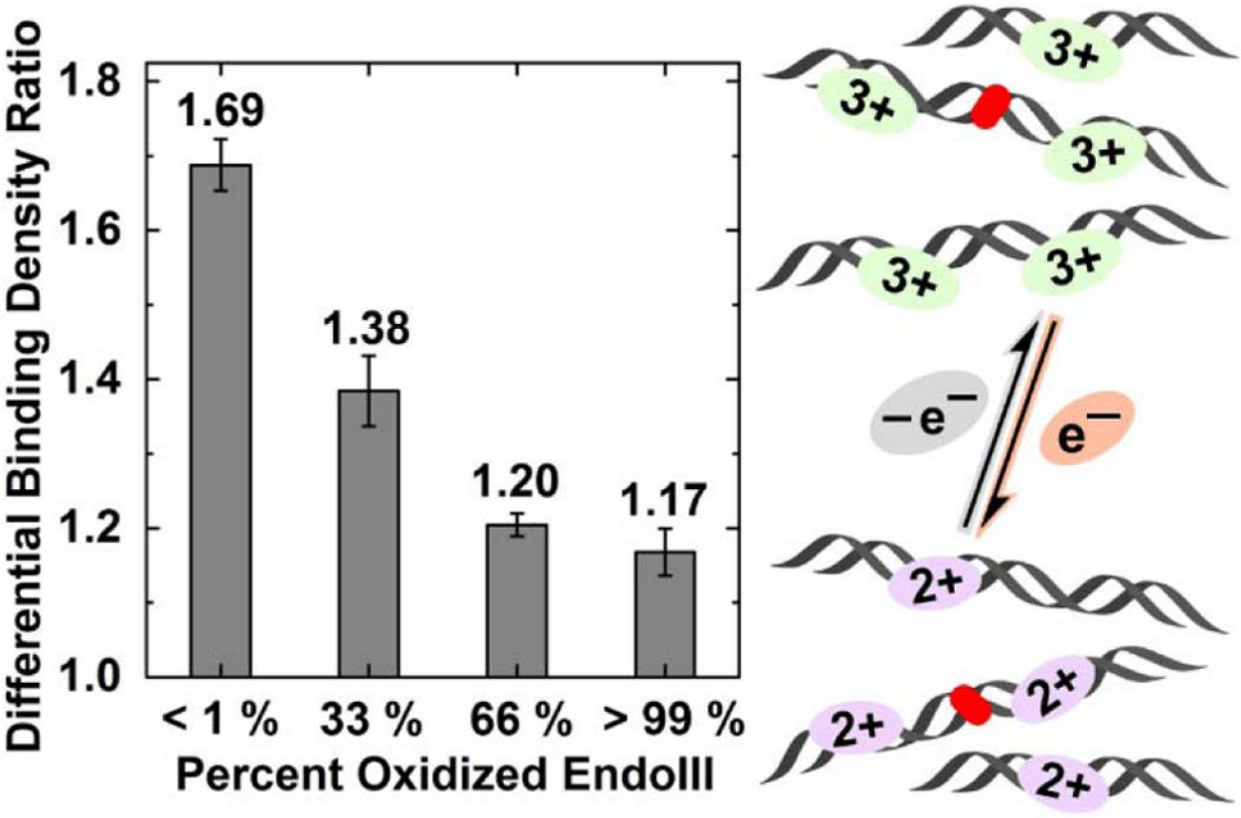

Figure 4.

AFM redistribution assay of EndoIII samples oxidized to various extent. The 33% and 66% oxidized EndoIII samples were prepared by mixing reduced and oxidized EndoIII in a 2:1 and 1:2 ratios, respectively. In the schematic on the right, short curved lines, long curved lines, and long curved lines with a red feature in the middle represent short well-matched DNA duplexes, long well-matched DNA duplexes, and long DNA duplexes with a C:A mismatch engineered in the middle.

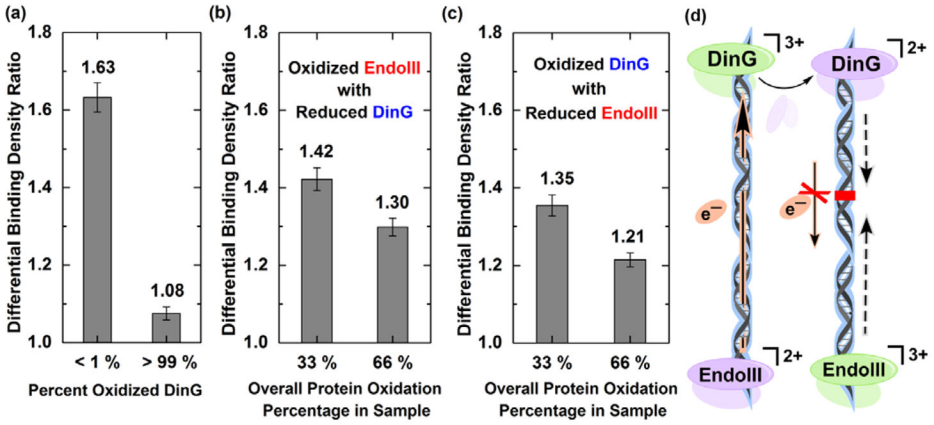

Figure 5.

AFM redistribution assays for (a) oxidized and reduced DinG, (b) oxidized EndoIII with reduced DinG, and (c) oxidized DinG with reduced EndoIII. The 33% and 66% oxidized samples in (b) were prepared by mixing reduced DinG and oxidized EndoIII in a 2:1 and 1:2 ratios, respectively. The 33% and 66% oxidized samples in (c) were prepared by mixing reduced EndoIII and oxidized DinG in a 2:1 and 1:2 ratios, respectively. (d) Our proposed DNA damage search model for DNA-processing enzymes carrying redox-active [4Fe4S] clusters that uses DNA-mediated CT as the first step of damage detection. Reduction of the [4Fe4S] cluster through unperturbed WM DNA allows for proteins to release from the DNA and search elsewhere for damage. If, however, damage is present along the DNA, the protein will not be reduced and will localize in the vicinity of the DNA damage.

Table 1

Binding affinity measurements of EndoIII to 21-mer dsDNA in the reduced and oxidized forms using MST, ITC, and EMSA.

Method	K_D (Red)	K_D (Ox)	$\frac{K_D\,(Red)}{K_D\,(Ox)}$
MST	6.1 ± 0.9 μM	0.011 ± 0.002 μM	550 ± 130
ITC	3.3 ± 0.4 μM	0.12 ± 0.03 μM	28 ± 8
EMSA	19 ± 2 μM	5.9 ± 0.3 μM	3.2 ± 0.3

K_D (Red) and K_D (Ox) denote the DNA-binding affinities of proteins with $[4Fe4S]^{2+}$ and $[4Fe4S]^{3+}$ clusters, respectively. Variations in K_D obtained across the three techniques are likely due to differences in experimental conditions. (see S.I. for further discussion) DNA buffer (pH 7.0, 5 mM NaH_2PO_4, 50 mM NaCl) was used for all cases with the following modifications: for MST 0.05% Tween 20 was added and for EMSA 20% glycerol was added. The buffer ionic strength in all three cases was kept constant. MST was carried out at 21–24 °C using wax-sealed capillary tubes, ITC was conducted at 21 °C in air, and EMSA was conducted at 4 °C in an anaerobic glove bag. N > 3 for all three methods.